



Experimental and numerical studies on the behavior and retaining mechanism of anchored stabilizing piles in landslides

Chengtang Wang¹ · Hao Wang¹ · Weimin Qin¹ · Hunan Tian¹

Received: 15 March 2021 / Accepted: 30 July 2021 / Published online: 8 September 2021
© Springer-Verlag GmbH Germany, part of Springer Nature 2021

Abstract

Anchored stabilizing piles (ASPs) are now extensively applied as an effective method in landslide treatment, but systematic studies ASPs in landslides are still lacking. The behavior of the ASPs in landslide during progressive loading was analyzed through a 1:50 similitude ratio model test, including the earth pressure, bending moment, shear force, distributed load, and anchor tension. Furthermore, a validated numerical model by the model test results in terms of the pile bending moment, anchor tension, and earth pressures behind the pile was utilized to conduct a parametric study of ASPs, including the embedded lengths of the pile, initial prestress of the anchor, and number of anchor levels. The results show that the landslide thrust distribution behind the piles changes from a rectangular shape to a parabolic shape with a large top and a small bottom during landslide evolution. The maximum positive bending moment occurs near the sliding surface. The variations in maximum positive bending moment and anchor tension all show three distinct phases: stable, rapid growth, and slow increase. The combined retaining mechanism of the stabilizing piles and anchor can be summarized as follows: the landslide thrust is mainly carried by the pile initially, and the anchor tension is gradually mobilized with increasing earth pressure to share the landslide thrust together with the pile and transferred to stable bedrock to ensure the stability of the landslide. The findings of this work are helpful for verifying and improving the present design of ASPs in landslide treatment.

Keywords Landslide · Anchored stabilizing piles · Model test · Numerical analysis · Combined retaining mechanism · Parametric study

Introduction

Landslides occur frequently all over the world and have caused great losses (Jian et al. 2014; Paronuzzi et al. 2013; Tang et al. 2019). To mitigate this kind of geological disaster, various protection measures have been developed (Wu et al. 2011; Zhao et al. 2017). Among the various protection measures, stabilizing piles have been proven to be an effective measure and have been extensively used to stabilize landslides (Kahyaoglu et al. 2017; Lirer 2012; Song and Cui 2016; Song et al. 2012). However, although the common stabilizing pile (CSP) has many advantages over other stabilization measures, it also has disadvantages including an excessive stress concentration effect near the sliding shear

zone and a limited horizontal bearing capacity and stiffness (Zhao et al. 2017). To overcome the above shortcomings, an anchored stabilizing pile (ASP) is formed by adding one or more anchor levels on the CSP. Compared with the CSP, the retaining performance is substantially improved, and larger landslide thrusts can be resisted. However, due to the complex coupling relationship among the landslides and the stabilizing piles as well as prestressed anchor cables, the design theory for ASPs in reinforcing landslides is still not mature, with no available technical code or specification that can be referred (Cai 2017; Wang et al. 2020; Wu et al. 2015). Consequently, the current engineering practice for ASP design still largely relies on experience, which cannot accurately reflect its actual mechanical characteristics and thus restricting its further engineering applications to a large extent.

Currently, many studies have been conducted on landslide-CSPs, involving the pile-soil interaction mechanism (Chen and Martin 2002; Ghasemzadeh et al. 2018; Zhang et al. 2017), the lateral force acting on the piles (Dai 2002; He et al. 2015; Tang et al. 2014; Zhou et al. 2014), the

✉ Hao Wang
hwang@whrsm.ac.cn

¹ State Key Laboratory of Geomechanics and Geotechnical Engineering, Institute of Rock and Soil Mechanics, Chinese Academy of Sciences, Wuhan 430071, Hubei, China

behavior of the stabilizing piles (Lirer 2012; Liu et al. 2021; Smethurst and Powrie 2007; Song et al. 2012; Zhang et al. 2018), and the failure mechanism of landslide-piles systems (He et al. 2020; Hu et al. 2019; Liu et al. 2020) utilizing various methods, such as numerical simulations, field measurements, and model tests. Among the aforementioned methods, physical model testing is an effective method for studying landslide evolution and the behavior of stabilizing piles, as it can reproduce the process of landslide occurrence and characterize landslide information in an inherently natural way (He et al. 2018; Jia et al. 2009; Li et al. 2018; Ling and Ling 2012; Liu et al. 2020; Shen et al. 2017). For instance, Guo and Qin (2010) investigated the behavior of vertically loaded free-head piles in sand subjected to lateral soil movements by a series of laboratory tests. The evolutionary and distribution characteristics of the soil pressure behind the piles were obtained through a model test by Tang et al. (2014). Li et al. (2016) developed an experimental apparatus to investigate the behavior of stabilizing piles in landslides with upper hard and lower weak bedrock.

Moreover, some field or laboratory tests have also been performed on the behavior of anchored sheet pile wall structures regarding the seismic response (Huang et al. 2020a; Ma et al. 2019; Qu et al. 2018; Zekri et al. 2015) and the deformation and mechanical characteristics (Tan et al. 2018; Zhao et al. 2019a, b). Ma et al. (2019) investigated the effectiveness of two different pile structures inside reinforced slopes by shaking table tests and found that prestressed anchor slab-pile walls can better support the slope than constrained anti-slide piles under similar shaking conditions. Zhao et al. (2019b) studied the behavior of anchored sheet pile walls during the excavation and backfilling construction process. Additionally, some scholars have also adopted numerical analyses to study the behavior of anchored sheet pile walls under static and dynamic conditions (Bilgin 2010; Degrande et al. 2002; Gazetas et al. 2016; Huang et al. 2020b). However, the mechanical behavior of ASPs is different from that of anchored sheet wall structures to some extent because of the effect of the sheet. Moreover, in contrast to the anchored sheet pile walls in high-fill slopes or excavation support

systems, the lateral earth pressure carried by the ASPs during landslide evolution is more complex. Accordingly, the findings from the research of anchored sheet pile walls cannot be directly applied to ASPs.

To summarize, the abovementioned field or model tests (including centrifuge tests) and numerical analyses have mainly focused on the behavior of CSPs in landslides (Lirer 2012; Song and Cui 2016; Zhang et al. 2018; Zhong et al. 2020) or the performance of anchored sheet pile walls applied in high-fill slopes, excavation support systems, embankment stabilization, and water front structures (Bilgin 2010; Gazetas et al. 2016; Huang et al. 2020b; Tan et al. 2018; Zhao et al. 2019a). In comparison, few studies have been conducted on the deformation and mechanical behavior of ASPs in landslides, and only a few relevant field engineering cases can be found (Kang et al. 2009). Actually, the ASPs in landslides may exhibit a more complicated response due to the complexity of the structural system and the dynamic characteristics of landslide evolution, and many issues regarding the mechanism of ASPs in landslides are still not completely understood. Hence, the behavior and retaining mechanism in landslides urgently need to be systematically investigated.

The objective of this paper is to study the behavior and retaining mechanism of ASPs during landslide evolution. To this end, a model test of the ASPs in landslides subjected to a stepwise thrust load on the rear of the model was conducted. The strain in the piles and anchor tension, as well as the earth pressure behind and in front of the piles during progressive loading, were measured and analyzed. In addition, a validated numerical model based on model test results was utilized to conduct the parametric study of ASPs, including the embedded lengths of the pile, initial prestress of the anchor cable and number of anchor levels. Furthermore, a comparison was made with the results from a model without an anchor via numerical analysis. Finally, the behaviors of the ASPs in relation to the thrust load were further analyzed and discussed to reveal the combined retaining mechanism of the stabilizing piles and prestressed anchor cable. The

Fig. 1 Model test arrangement of the landslide-anchored stabilizing pile system: **a** schematic diagram of the model test system; **b** the actual model test system

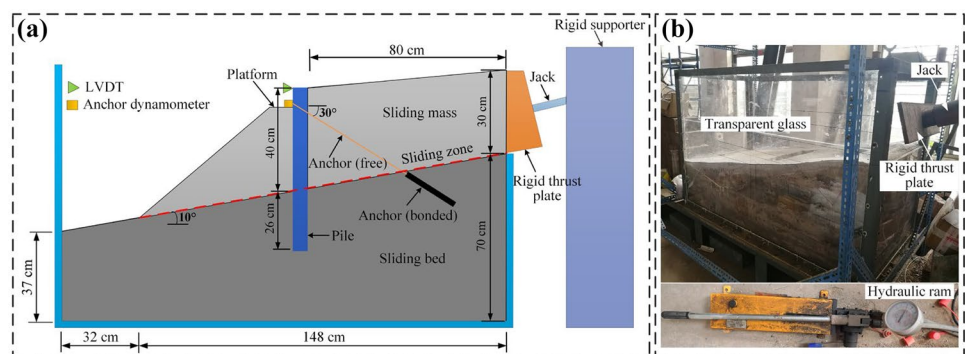


Table 1 Mechanical properties of the soil in the sliding mass and sliding zone

Object	Material	Unit weight (kN/m ³)	Cohesion (kPa)	Friction (°)	Young's modulus (MPa)
Prototype	Sliding mass	21.14	N/A	N/A	300
	Sliding zone	21.14	16–18	17–19	100
Model	Sliding mass	20.0	10.5	22.9	4
	Sliding zone	19.2	8.4	22.6	3.8

findings of this work are helpful for verifying and improving the present design of ASPs in landslide treatment.

The remainder of this paper is organized as follows: In “Experimental design and scheme,” the experimental design and scheme are briefly introduced. “Test results and analysis” presents the test results and analysis. Numerical analysis results are described in “Numerical analysis.” “Discussion” discusses the differences in pile deflection and evolution law of the safety factor between the landslide-ASP and landslide-CSP models, as well as the combined retaining mechanism of the stabilizing piles and prestressed anchor cable. Conclusions and future studies are given in “Conclusions and future studies.”

Experimental design and scheme

Landslide model and materials

The geological and engineering scenario of typical colluvial landslides in the Three Gorges Reservoir area was taken as the prototype in this test. Moreover, since the focus of this study is mainly on the behavior and retaining mechanism of ASPs, a half landslide model test was adopted (Tang et al. 2014). A half landslide model means that the study area considered in the model test is part of the prototype landslide, rather than the entire prototype landslide. A physical model of a landslide reinforced with ASPs was constructed with a 1:50 similitude ratio, and the cross-sectional geometry of the model is shown in Fig. 1a. This physical model consists of a

sliding mass, sliding zone, sliding bed, modeling piles, and prestressed anchor cable (see Fig. 1a). The landslide models are 180 cm, 80 cm, and 100 cm in length, width, and height, respectively. The thickness of the sliding zone is 2 cm, with a slope angle of 10°. Four modeling piles were installed in the landslide model, and the anchor was installed at the modeling pile 8 cm away from the pile head. In addition, for the convenience of installing the anchorage and anchor dynamometer as well as the tensioning of the anchor, a platform was set in front of the pile (see Fig. 1a).

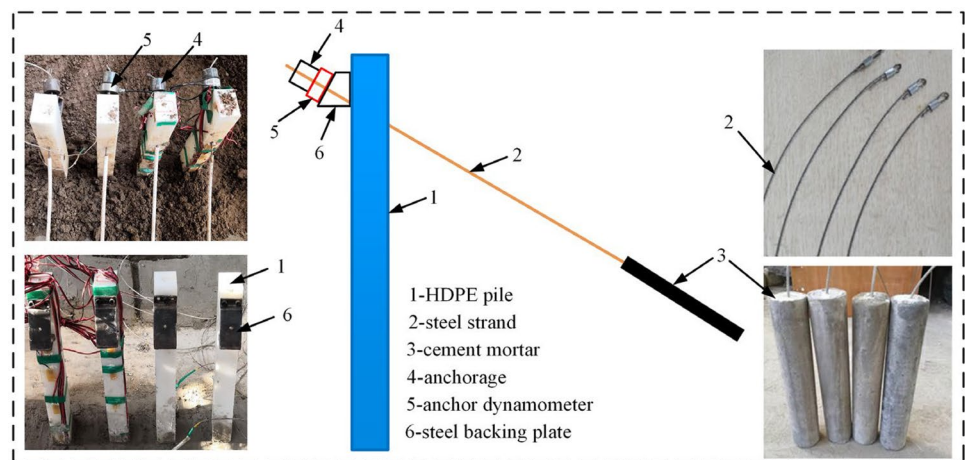
According to the similarity between the physical model and the prototype, the final material ratio of the sliding mass and sliding zone was determined by the orthogonal mix proportion test. The sliding mass is made of a mixture comprising clay (48.4%), standard sand (38.8%), bentonite (0.9%), and water (11.9%), and the sliding zone is composed of clay (66%), standard sand (22%), and water (12%). The sliding bed is regarded as stable bedrock, which is made of bricks, and the cement mortar is coated on its surface. The physical and mechanical parameters of the materials obtained through the laboratory soil tests are shown in Table 1. The parameters of the materials in the prototype obtained from research results of the Majiagou landslide in the Three Gorges Reservoir area (He et al. 2018).

High-density polyethylene was employed to manufacture the pile. The lengths of the cantilever and embedded section of the pile are 40 and 26 cm, respectively. The pile cross section is 4 cm × 6 cm. The pile center-to-center distance is 12 cm. The lengths of the free and bonded sections of the anchor are 50 and 25 cm, respectively. The dip angle of

Table 2 Parameters and similitude ratios of the prototype and model of the ASP structure

Object	Parameters	Prototype	Model	Similitude ratio	
				In theory	In practice
Pile	Pile cross section	2 m × 3 m	4 cm × 6 cm	50	50
	Cantilever length	13 m	40 cm	50	33
	Embedded length	9 m	26 cm	50	35
	Pile center-to-center distance	7 m	12 cm	50	58
Anchor cable	Total length	24 m	75 cm	50	32
	Anchor diameter	150	3	50	50
	Anchorage ratio	2	2	1	1
	Anchorage angle	30°	30°	1	1

Fig. 2 Schematic diagram and actual model showing the internal structure of the anchored stabilizing pile



anchor is 30° . The free section of the anchor was simulated using a 3-mm diameter steel strand, and the bonded section of the anchor is made of M20 cement mortar. The parameters and similitude ratios of the prototype and model of the ASP are listed in Table 2.

To simulate a pretension system, the steel strand passes through two narrow holes on the modeling pile and a steel backing plate. The steel strand was tensioned by the pre-defined load, and then was fixed by a self-made anchorage (see Fig. 2).

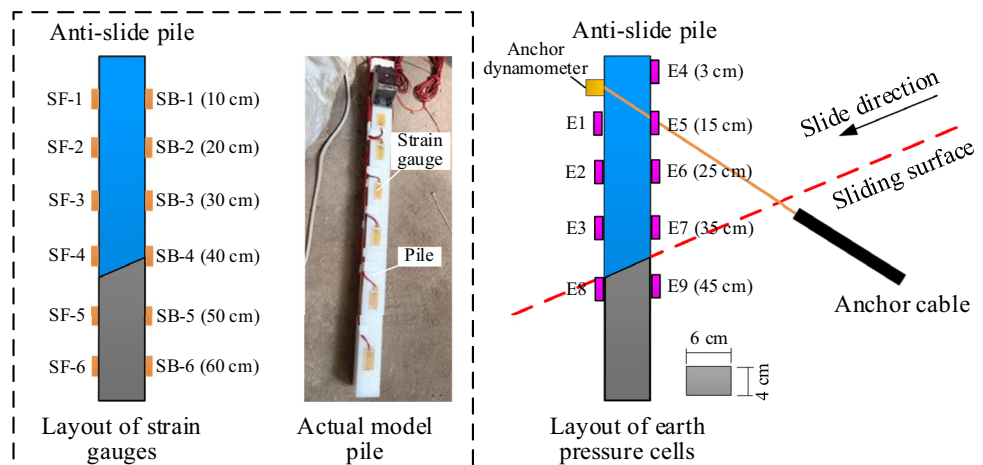
Loading and monitoring system

The loading system consists of a jack, hydraulic ram, and rigid thrust plate, which were used to achieve the infliction and transmission of the driving force, as shown in Fig. 1b. In addition, the rigid thrust plate was designed to move downward at an inclination of 10° , which was parallel to the sliding direction. Step loading with a 0.6-kN increment was applied to the rear of the model to simulate the thrust loads from the upper part of the landslide, which has been

adopted by other researchers (He et al. 2018; Tang et al. 2014; Zhou 2020). Moreover, the load should be maintained for a certain period of time after each step of thrust load was applied to ensure that the monitored data of all sensors were stable. Afterwards, the next loading step was applied. These processes continued until the landslide model fails.

To analyze the behavior of the ASPs under progressive loading, 9 earth pressure cells were distributed on the uphill and downhill sides of the piles, and 12 strain gauges were symmetrically installed on the external surface of the piles. The arrangement of earth pressure cells and strain gauges is shown in Fig. 3. Strain gauge measurements were used to calculate the bending moment in the piles. LVDTs were attached to the pile head to record the lateral displacement at the pile head (see Fig. 1a). Furthermore, an anchor dynamometer was installed on the external anchor head to monitor the variation in the anchor tension during progressive loading. All readings through electrical signals were recorded and digitized with a data acquisition system.

Fig. 3 Arrangement of earth pressure cells and strain gauges



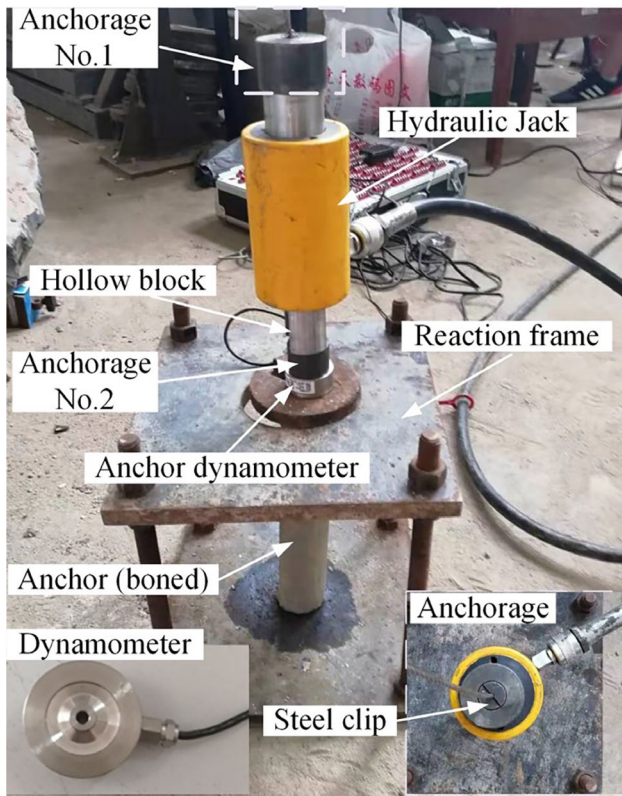


Fig. 4 Photos of the prestressed loading device and jack calibration test

Experimental procedures

The main procedures of the model test are as follows:

- The sliding bed (bedrock) was made using bricks, and the cement mortar was coated on its surface. The embedded section of modeling piles and the bonded section of anchor cables were installed in the bedrock.
- Silicone grease was applied at the sidewalls before back-filling the model box to reduce the boundary effects. The soil of the sliding mass was filled into the box layer by layer with a 100-mm thickness of each layer using the controlled-volume method (Lin and Wang 2006). The

required soil weight for each layer was calculated based on the target density (2.0 g/cm³). Meanwhile, earth pressure cells were installed on both sides of the piles during the process of filling soil layer by layer.

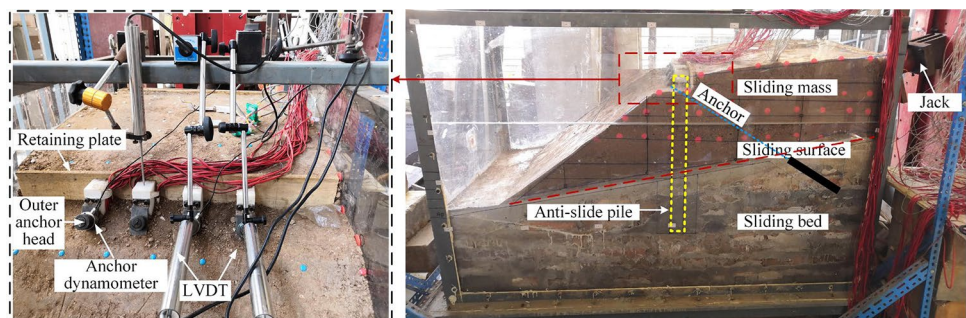
- The prestressed anchor cable was tensioned by a self-developed loading device (Fig. 4), and was finally prestressed to 200 N, which was equal to 500 kN in the prototype. The initial prestress load of the anchor cables were applied according to the following steps: First, the steel strand of the free section of the anchor was passed from the narrow holes of the reaction frame, anchor dynamometer, No. 2 anchorage, hollow cushion block, jack, and No. 1 anchorage in turn (Fig. 4), and the anchor dynamometer was connected to the acquisition instrument. Second, the steel clip was pressed into the No. 1 anchorage to fix the steel strand above the jack, and the steel clip was now not pressed into the No. 2 anchorage to ensure that the steel strand between the jack and the bonded section of the anchor is in a relaxed state. After that, the steel strand was tensioned by the predefined load, and was fixed by driving the steel clip into the No. 2 anchorage. Finally, the jack and No. 1 anchorage were withdrawn from the loading device, and the tensioning and locking of the initial prestress of the anchor was now finished.
- The hydraulic jack and the rigid thrust plate were installed on the rear of the model.
- The initial data of all sensors were set to zero. Then, step loading was applied to the rear of the model in light of the aforementioned loading scheme, and the monitored data are recorded.

According to the above experimental procedures, the final model of the landslide-ASP system and the sensor layout are shown in Fig. 5.

Test results and analysis

In this section, the measured earth pressure, strain in the piles, and anchor tension under progressive loading are provided and analyzed to investigate the behavior and

Fig. 5 The final model of the landslide-anchored stabilizing pile system and the sensor layout



retaining mechanism of ASPs during landslide evolution. Specifically, the following analyses were performed in terms of the variation in the earth pressure distribution behind and in front of the piles, bending moment, shear force and distributed load in the piles, as well as anchor tension.

Earth pressure distribution along the piles

The shape and distribution of the lateral force acting on the pile are critical factors in the design of an ASP, thus were measured and analyzed in our study. The monitored earth pressure distributions behind and in front of the piles with different levels of thrust load are shown in Figs. 6 and 7, respectively. Because of the earth pressure cells' failure at E_8 and E_9 (see Fig. 3), the earth pressure on the pile in the bedrock was not recorded; as a result, the following analyses mainly aimed at the earth pressure distribution along the cantilever section of the pile above the sliding surface, where the positive value of the earth pressure denotes the landslide thrust (the earth pressure behind the pile) and the negative value of the earth pressure represents the earth resistance (the earth pressure in front of the pile).

As shown in Fig. 6, the landslide thrust generally increases gradually with increasing thrust load. When the thrust load was less than or equal to 7.8 kN, the landslide thrust behind the pile was distributed approximately in a rectangular shape, and the location of the maximum value of earth pressure was at a depth of 20 cm (between E_5

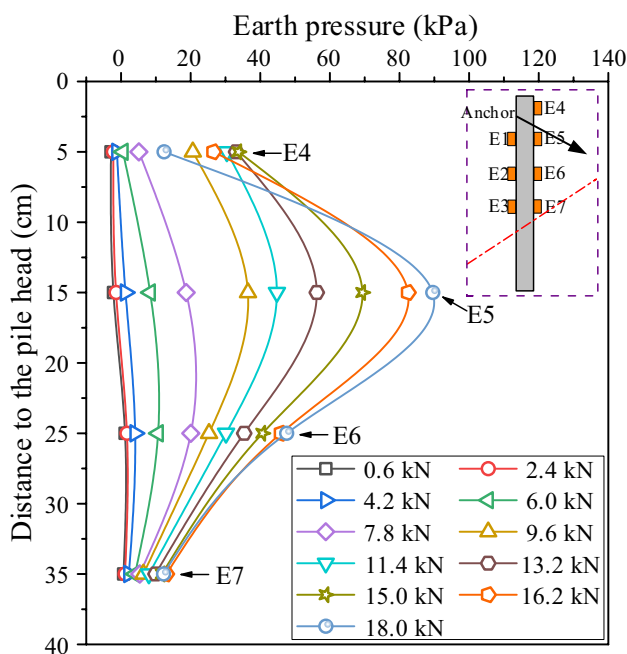


Fig. 6 Earth pressures behind the pile

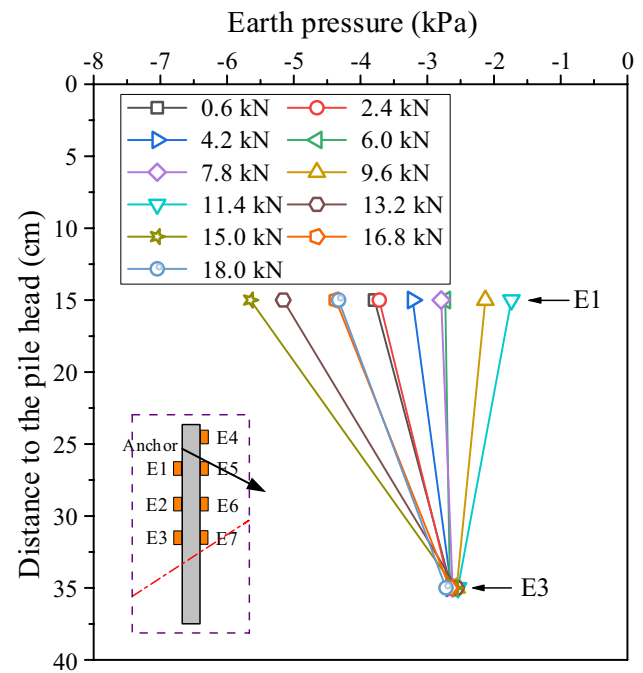


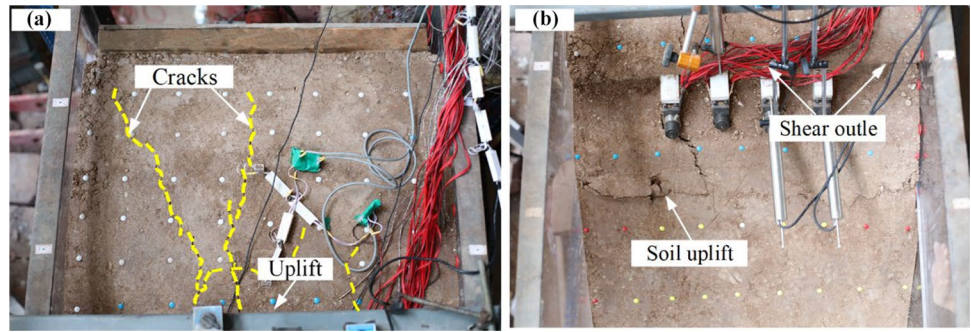
Fig. 7 Earth pressures in front of the pile

and E_6). When the thrust load was greater than 7.8 kN, the landslide thrust distribution changed from a rectangular shape to a parabolic shape with a large top and a small bottom, and the position of the maximum value of the earth pressure shifted to a depth of 15 cm (E_5) and reached its maximum value of 89.5 kPa at a final thrust load of 18.0 kN. Furthermore, it can also be found that the resultant force action point of the landslide thrust moved upward as the thrust load was over 7.8 kN. The reason for the upward shift in the location of the maximum landslide thrust is that the inverse pulling effect of the anchor cable on the pile gradually increased as the thrust load increased, causing a stress concentration in the nearby soil at the anchor cable and resulting in an increase in the earth pressure at E_5 , while the earth pressure cell at E_5 was located near exactly where the anchor cable was set.

In addition, it is clear that the earth pressure at E_4 declines abruptly at the thrust load of 18.0 kN, and this phenomenon is induced by the deflection of the earth pressure cell due to soil movement and upheaval (He et al. 2018). Moreover, cracks and soil uplift can be observed in the landslide model surface near E_4 , as shown in Fig. 8a, and it can be observed that the earth pressure at E_7 was very small during the entire testing procedure, which may be caused by the friction between the sliding mass and sliding zone.

As illustrated in Fig. 7, due to the earth pressure cells' failure at E_2 , the value of earth pressure at E_2 was not included in Fig. 7. It is clear that the earth pressures at E_1 gradually are increased with increasing thrust load, while

Fig. 8 Landslide model surface deformation: **a** behind the piles and **b** in front side of the piles



the earth pressures at E_3 remains almost unchanged. During the whole progressive loading process, the corresponding maximum values of negative earth pressures at E_1 and E_3 are -5.6 and -2.6 kPa, respectively. Additionally, it is clear that the value of the earth resistance is very small compared with that of the landslide thrust, this is because the earth resistance is induced by compressing the soil in the front side of the pile due to the deflection of the piles, while the pile deformation is restricted effectively by the anchor. Consequently, the anti-sliding effect of ASPs can effectively reduce the transmission of stress from the thrust plate to the soil at the front side of the pile, contributing to the stability of the sliding mass in front of the pile (see Fig. 8b). Furthermore, the result also illustrates that the earth resistance can be negligible (or as a safety reserve) in the design of an anchored stabilizing pile in landslides, especially for the condition of an unstable sliding mass existing at the front side of the pile.

Internal forces in the piles

To evaluate the pile behavior in ASP structures during landslide evolution, the internal forces in the piles involving the bending moment, shear force, and distributed load along the piles were investigated.

The bending moment can be calculated by strain measurements as follows (Lirer 2012; Zhang et al. 2018):

$$M = \frac{EI(\epsilon^+ - \epsilon^-)}{a} \tag{1}$$

where M is the bending moment in the pile, EI represents the bending stiffness of the pile, ϵ^+ and ϵ^- correspond to the strain measurements at the uphill and downhill sides of the pile, respectively, and a denotes the distance between two strain gauges.

The shear force in the pile can be obtained by the derivations of the bending moment as follows:

$$F(x) = M'(x) = \lim_{h \rightarrow 0} \frac{M(x_i + h) - M(x_i)}{h} \tag{2}$$

where x_i represents the depth of the strain gauges. If h is small enough, then a centered difference formula can be utilized to approximate the derivative (Hu et al. 2019):

$$F(x) = \lim_{h \rightarrow 0} \frac{M(x_i + h) - M(x_i - h)}{2h} \tag{3}$$

In general, there is a lack of sufficient data to calculate an accurate derivative of a single point in practice. Thus, we treated discrete data utilizing the centered difference formula and computed the derivative at point M_i by taking the average of the slopes between the point and its two closest neighbors (Hu et al. 2019).

Hence, the derivative function used to discrete data points can be denoted as

$$F(x) = \frac{1}{2} \left(\frac{M_{i+1} - M_i}{x_{i+1} - x_i} + \frac{M_i - M_{i-1}}{x_i - x_{i-1}} \right) \tag{4}$$

Similarly, the density of the distributed load on the pile can be computed by the derivations of the shear force, as shown in Eq. (5).

$$q(x) = \frac{1}{2} \left(\frac{F_{i+1} - F_i}{x_{i+1} - x_i} + \frac{F_i - F_{i-1}}{x_i - x_{i-1}} \right) \tag{5}$$

The bending moment distribution along the piles with different levels of thrust load is illustrated in Fig. 9. The positive and negative values of the bending moment denote the tensile strain on the external surface of the piles on the uphill and downhill sides of the piles, respectively. Generally, all curves of the bending moment distribution under each level of thrust load are approximately S-shaped, which is significantly different from that of the bending moment distribution obtained from the model experiment of a landslide reinforced by a common stabilized pile (Hu et al. 2019; Li et al. 2016). Moreover, it is clear that the maximum value of the positive bending moment occurred near the sliding surface, which is also observed for real ASPs in practical engineering (Kang et al. 2009).

Furthermore, the variation in the bending moment value with the thrust load shows three distinct phases: At the

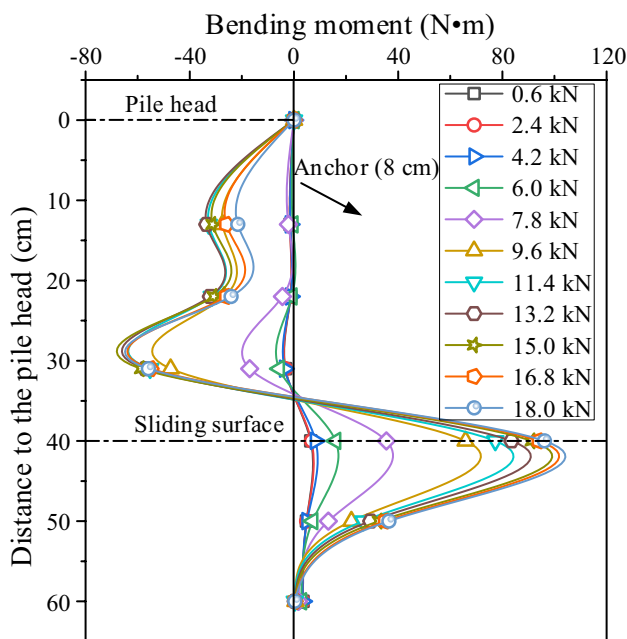


Fig. 9 Bending moment distribution along the piles

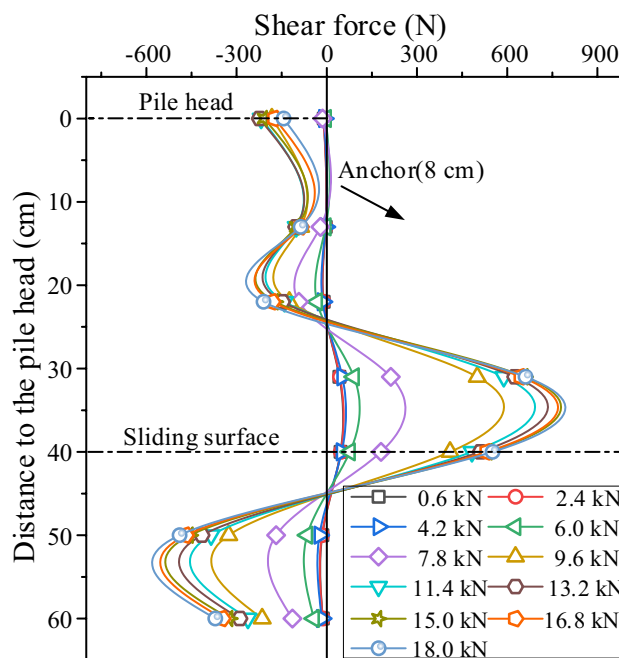


Fig. 10 Shear force distribution along the piles

initial loading stage, the bending moments of each monitoring point were small because the pile itself did not undergo much deformation as the thrust loading is mainly consumed in the compaction process of the soil behind the pile. As the thrust load is further increased, the redundant thrust load is gradually transferred from the rear part of the sliding mass to the piles, and the bending moment of the piles increase dramatically, especially when the thrust load is increased from 6.0 to 9.6 kN. Additionally, the maximum value of the positive bending moment is increased from 15.98 to 65.83 Nm. When the thrust load is greater than 9.6 kN, the increase rate of the maximum bending moment starts to decrease gradually.

Figure 10 shows the calculated shear force distribution of the pile at different levels of thrust load according to Eq. (4). It can be observed that the variation in the shear force value shows a similar trend with the variation in the bending moment value under progressive loading. The maximum positive shear force was up to 760 N, located at a depth of 35 cm (near the sliding surface), and the minimum negative shear force was up to -605 N, located at a depth of 54 cm. This result demonstrates that the landslide thrust above the sliding surface is carried by the stabilizing piles and is transferred to the stable bedrock, thus ensuring the stability of the system. In addition, it can be seen that the shear force in the pile ranges from 5 to 15 cm and shows a concave shape, which may be attributed to the inverse pulling effect of the anchor.

The calculated distributed load along the pile at different levels of thrust load according to Eq. (5) is presented in

Fig. 11. For the cantilever section of the pile, the distributed load behind the pile shows an approximately parabolic distribution, peaking at a depth of 27 cm. The earth resistance in front of the pile is very small compared with the landslide thrust behind the pile, which is consistent with the aforementioned observation results for the earth pressure along the

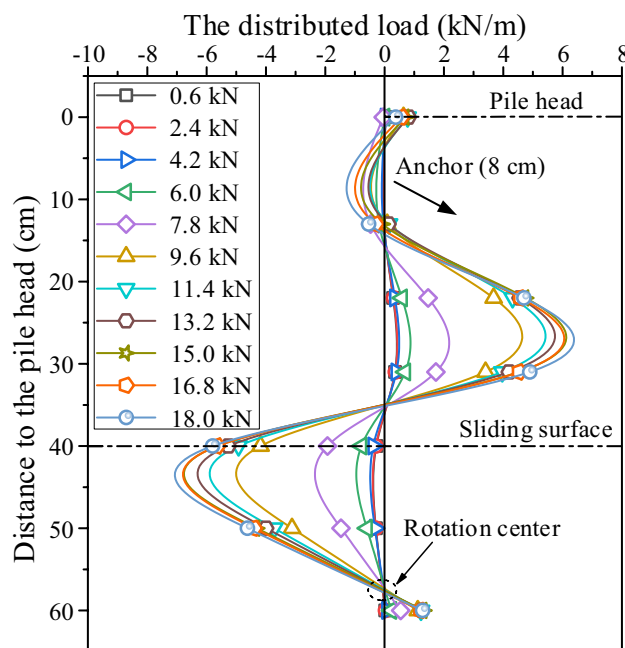


Fig. 11 The distributed load along the piles

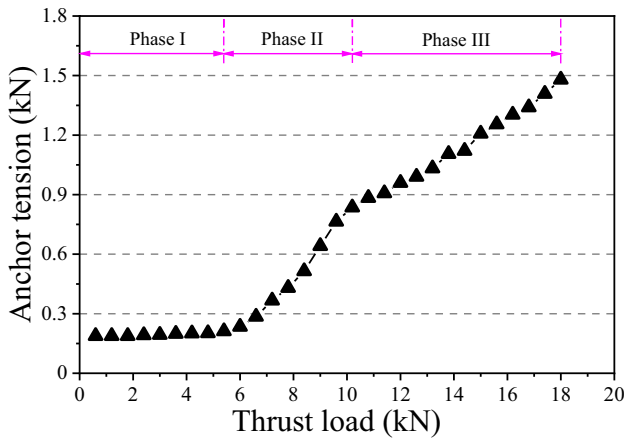


Fig. 12 The variation curve of the anchor tension during progressive loading

pile. This finding might be attributed to the inverse pulling effect of the anchor cable on the pile. For the embedded section of the pile, the distributed load on the pile shows an approximately inversed triangular distribution, peaking near the sliding surface. Additionally, the rotation center of the pile below the sliding surface can be judged preliminarily from the diagram of the distributed load along the embedded section of the pile, and it is located at a depth of 58 cm (see Fig. 11). It can also be seen clearly that the pile resistance is mainly provided by the sliding bed at the front side of the pile (above the rotation center), while the earth resistance behind the pile is small and mainly distributed near the pile bottom (below the rotation center). This result indicates that the thrust load is transferred into the bedrock by the piles to maintain the stability of the landslide, which is in agreement with the results reported by Hu et al. (Hu et al. 2019).

Anchor tension analysis

Figure 12 shows the anchor tension versus the thrust load. The variation trend of the anchor tension is similar to that of the maximum positive bending moment in the pile. The

trend also shows three distinct phases. At the initial loading stage, the anchor tension remains almost unchanged and stable at the initial prestress load of 200 N. With further increasing thrust load, an apparent increment of the anchor tension occurs, in which the anchor tension increases rapidly from 200 to 800 N as the thrust load increases from 6.0 to 9.6 kN. When the thrust load is > 9.6 kN, the increase rate of the anchor tension begins to decrease slightly, and the anchor tension finally reaches 1479.6 N at the end of the tests. This result indicates that most of the thrust load was consumed in the compaction process of the soil between the pile and rigid thrust plate at the initial loading stage, thus the thrust load transferred to the pile was small. After that, the lateral earth pressures on the pile increase substantially after the soil was compacted by the continuing increase of the load on the thrust plate, and the anchor tension was gradually mobilized to share the landslide thrust with the pile.

Numerical analysis

In this section, the calibrations of the numerical model are performed first, followed by a parametric study, which may contribute to the design optimization of the ASP structures in landslides.

Establishment of the numerical model

A 3D numerical model of the landslide-ASP system was established using FLAC3D, as shown in Fig. 13. The identical model dimensions and boundary conditions used in the model tests were adopted in the numerical model. In the initial stress equilibrium stage, the full boundary constraint was applied to the bottom boundary of the numerical model, displacements along the directions normal to surfaces on four sides of the model were also fixed, and the boundary in the upper part is the free boundary. During the progressive loading stages, the displacement constraint boundary in the rear surface of the landslide mass of the model was removed, and the uniform thrust surface load same as that in the model

Fig. 13 Numerical model of a landslide-anchored stabilizing pile system

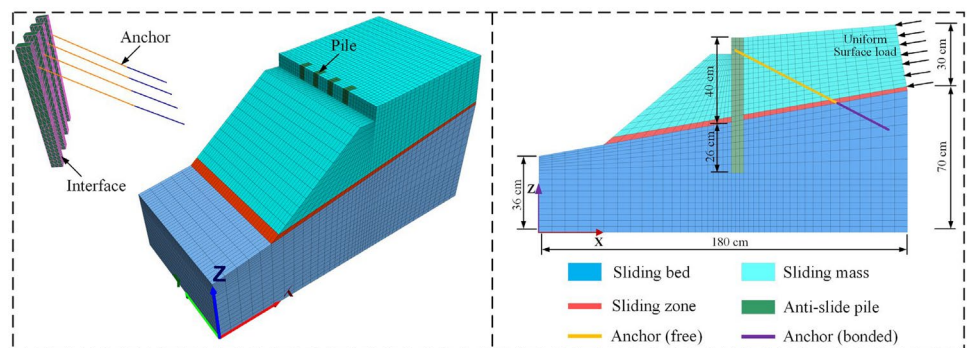


Table 3 Material properties adopted in the numerical model

Object	Unit weight (kN/m ³)	Young's modulus (MPa)	Poisson's ratio	Cohesion (kPa)	Friction (°)
Sliding mass	20.0	4.0	0.28	10.5	22.9
Sliding zone	19.2	3.8	0.28	8.4	22.6
Sliding bed	25	450	0.2	250	38
Stabilizing piles	9.5	1.4×10^3	0.2	N/A	N/A
Anchor cable	78	1.95×10^5	N/A	N/A	N/A

test is applied on the rear surface of the landslide mass of the model, as shown in Fig. 13. The stabilizing piles were modeled by an elastic constitutive model, and the soils in the landslide model were modeled by a standard Mohr–Coulomb constitutive model. The adopted material properties for calculations are listed in Table 3.

The cable structural element in FLAC3D was used to simulate the anchor of the ASP structure. The grout cohesive strength between the bonded section of the anchor and the bedrock was 0.25 MN/m, and the cohesive strength between the free section of the anchor and the soil was neglected.

To simulate the interaction behavior at the pile-soil interface, an interface was established between the pile and the soil. The main parameters of the pile-soil interface elements, as shown in Table 4, were determined based on the recommendation in the FLAC3D manual (ITASCA Consulting Group 2012), which is given below:

$$k_n = k_s = 10 \max \left(\frac{K + \frac{4}{3}G}{\Delta z} \right) \quad (4)$$

in which k_n and k_s denote the normal and shear stiffness of the interface, respectively; K and G are the bulk and shear moduli of the material connecting to the interface, respectively; and Δz represents the minimum size of the element in the normal direction. The K and G of the sliding mass are 3.03 and 1.56 MPa, respectively; the K and G of sliding zone are 2.88 and 1.48 MPa, respectively; the K and G of sliding bed are 175.78 and 340.91 MPa, respectively.

Model calibration

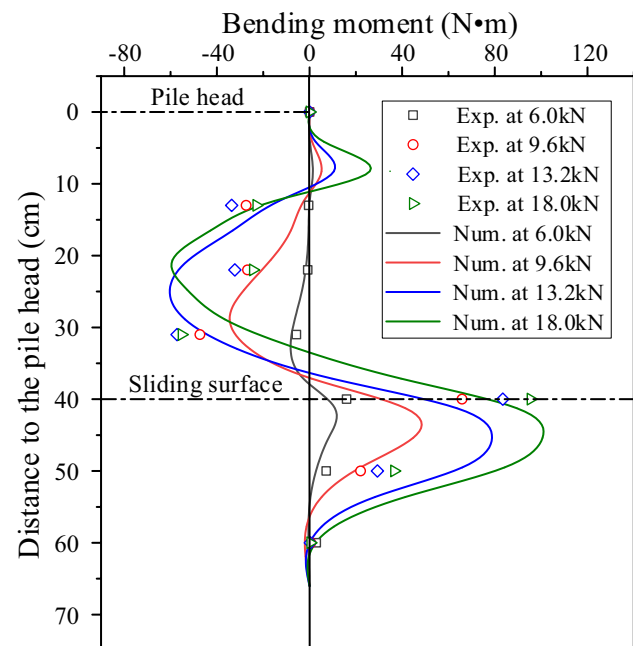
The bending moment in the pile, anchor tension, and earth pressures behind the pile obtained from the experiment were used to calibrate the numerical model established above. A comparison between the measured and simulated bending

Table 4 The main parameters of the pile-soil interface in the numerical models

Items	Normal stiffness (MPa)	Shear stiffness (MPa)	Cohesion (kPa)	Friction (°)
Interface	7330	7330	8.4	18.3

moments in the pile at a thrust loads of 6.0, 9.6, 13.2, and 18.0 kN are presented in Fig. 14. In both numerical calculations and model test, the bending moment distributions in the pile are all approximately S-shaped under each level of thrust load. Additionally, it is clear that the maximum value of the positive bending moment occurred near the sliding surface. In general, the numerical calculations are in good agreement with the experimental measurements. The significant difference between the value of bending moment obtained from numerical results and experimental data is mainly in the cantilever section of the pile, which is probably caused by the definitions of pile-soil interface parameters.

Figure 15 shows a comparison between the anchor tensions measured experimentally and calculated numerically. The variation curves of the anchor tension obtained from numerical analyses are generally consistent with the experimental results. Moreover, it is also clear that the significant difference between the measured and simulated values mainly occurred in the second phase of the anchor tension

**Fig. 14** Comparison of the measured and calculated bending moments in the piles

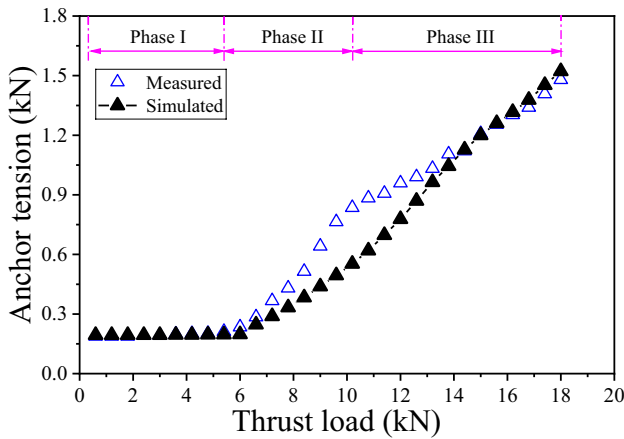


Fig. 15 Comparison of the measured and calculated anchor tension

curves (see Fig. 15) and that the simulated values are smaller than the measured values. This result may be caused by the soil uplifts and cracks in the model test, especially for the soil around the stabilizing piles and anchor, leading to the pile tilting outward, which cannot be reflected in the numerical calculation.

A comparison of the simulated and measured earth pressures behind the pile at a thrust loads of 6.0, 9.6, 13.2, and 18.0 kN are shown in Fig. 16. The distribution pattern of earth pressures behind the pile obtained by numerical calculations were generally the same with model test results. Moreover, the values of earth pressures determined by numerical simulation are in good agreement with that of model test, except for that the earth pressure at E_4 when thrust load is 18.0 kN. The earth pressure at E_4 declines abruptly at the thrust load of 18.0 kN in the experiment, this is induced by the deflection of the earth pressure cell due to soil movement and upheaval, while this cannot be well reflected in the numerical simulation.

In summary, the bending moment in the pile, anchor tension, and earth pressures behind the pile from the above two analyses are in reasonable agreement, which proves that the present numerical model is rational and effective for the analysis of the behavior of the ASPs in landslides.

Parametric study

The parametric study for several critical parameters in the design of the ASPs was carried out based on the above validated numerical model, including the embedded lengths of the stabilizing pile, the initial prestress of the anchor cable, and the number of anchor levels. The mechanical parameters, boundary, and loading conditions are identical to those of the numerical model described above. It is noted that due to the calculation of the landslide, CSP model (the number

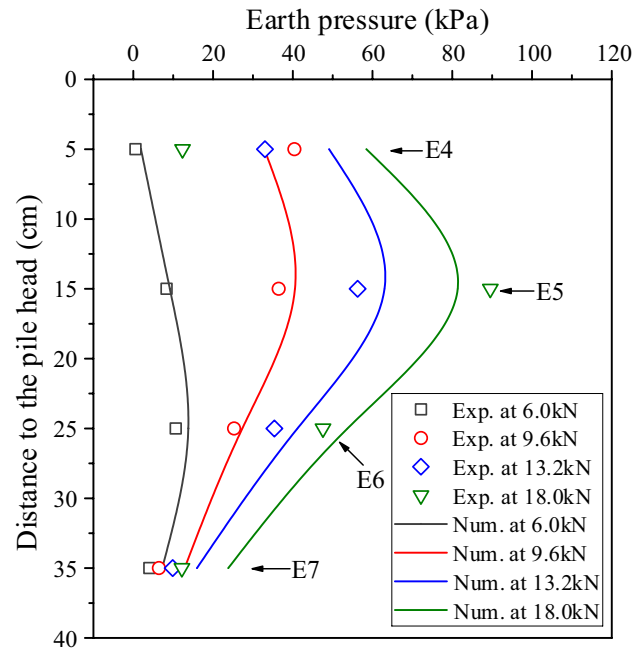


Fig. 16 Comparison of the measured and calculated earth pressures behind the piles

of anchor levels is 0) does not converge when the thrust load on the rear of the model is over 12.0 kN; thus, the following comparative analysis of pile deflection and bending moment are based on the calculated results at a load of 12.0 kN. The variables and their ranges considered in the parametric study are listed in Table 5.

Effect of the embedded lengths of stabilizing pile

Four ASPs with different embedded lengths of piles, i.e., 20 cm, 26 cm, 32 cm, and 38 cm, were simulated to investigate the effect of embedded lengths on pile deflection and bending moment. The variations in the deflections of piles with different embedded lengths of piles are presented in Fig. 17. The corresponding absolute value of lateral displacements at the pile heads of different embedded pile lengths (20 cm, 26 cm, 32 cm, and 38 cm) are 3.67 mm, 3.41 mm, 3.72 mm, and 4.04 mm, respectively. It is clear that there is a critical value (critical embedded length of piles) regarding the influence of the embedded length of piles on pile deflection. When the embedded length of the

Table 5 Variables and ranges adopted in the parametric study

Variable	Range
Embedded length of the pile	20 cm, 26 cm, 32 cm, 38 cm
Initial prestress of the anchor cable	0 N, 200 N, 400 N, 600 N
Number of anchor levels	0, 1, and 2

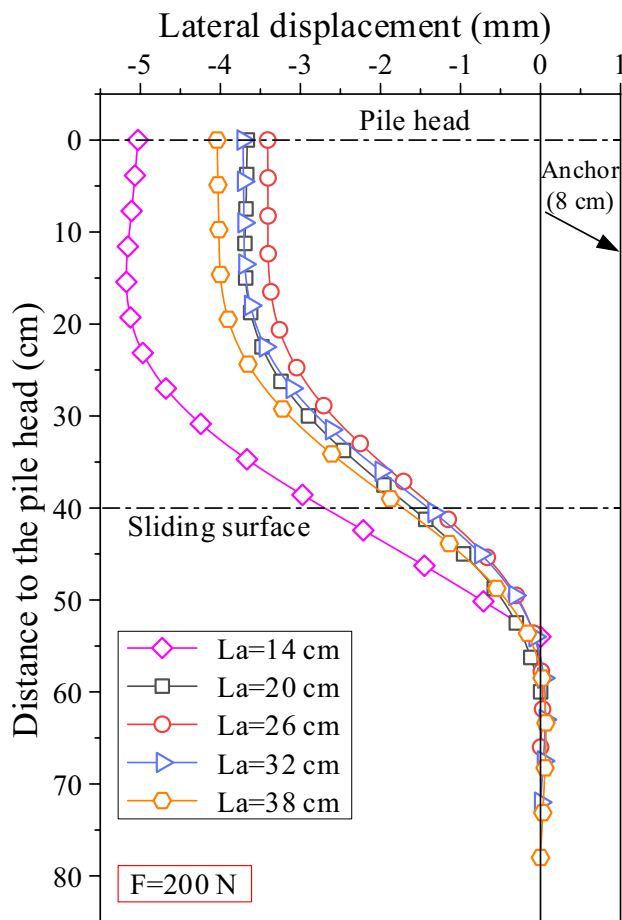


Fig. 17 Comparison of pile deflections with different embedded lengths of the pile

pile is smaller than the critical value, the pile deflection decreases as the embedded length of the piles increases. However, when the embedded length of the pile exceeds the critical value, the pile deflection increases as the embedded length of the piles increases. Figure 18 shows the variation in the bending moment along the pile with different embedded lengths of the pile. The bending moment of piles increases with the increase in the embedded length of the piles but with a small increment, which is in agreement with the results by Yang et al. (2011). The maximum values of the positive and negative bending moments increase by 13% and 9%, respectively, as the embedded length of the piles increases from 20 to 38 cm. The similar law of variation was also obtained by Xu and Huang (2021). Furthermore, it is seen that the bending moment of the pile tends to zero on the section of the pile near the bottom when the embedded length of the pile is 38 cm. This finding indicates that a longer embedded length is redundant and not conducive to achieving better economy.

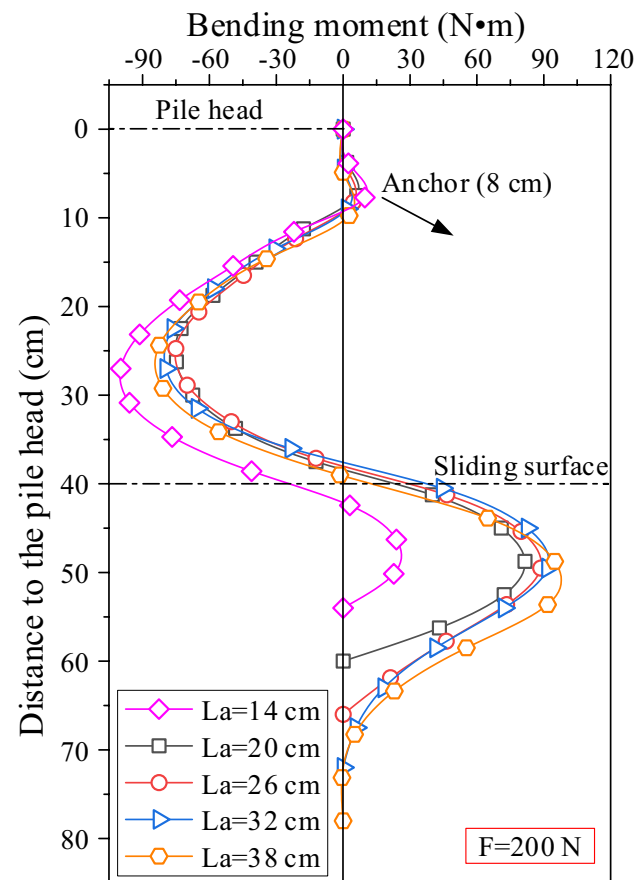


Fig. 18 Comparison of the bending moment in the piles with different embedded lengths of the pile

Effect of the initial prestress of the anchor cable

Four series of numerical models with identical properties and various initial prestresses of the anchor were performed to investigate the influence of the initial prestress of the anchor on the pile deflection and bending moment. The effects of the initial prestress of the anchor on the pile deflection and bending moment are shown in Figs. 19 and 20, respectively. As shown in Fig. 19, the pile deflection decreases almost linearly with increasing initial prestress of the anchor. The corresponding absolute value of lateral displacements at the pile heads with different initial prestresses of the anchor (0 N, 200 N, 400 N, and 600 N) are 3.77 mm, 3.41 mm, 2.99 mm, and 2.61 mm, respectively. The maximum deflection of the pile (lateral displacement at the pile head) is reduced by more than 31% when the initial prestress of the anchor increases from 0 to 600 N. This result indicates that the increase in the initial prestress of the anchor in a reasonable range can more effectively limit the deflections of the pile.

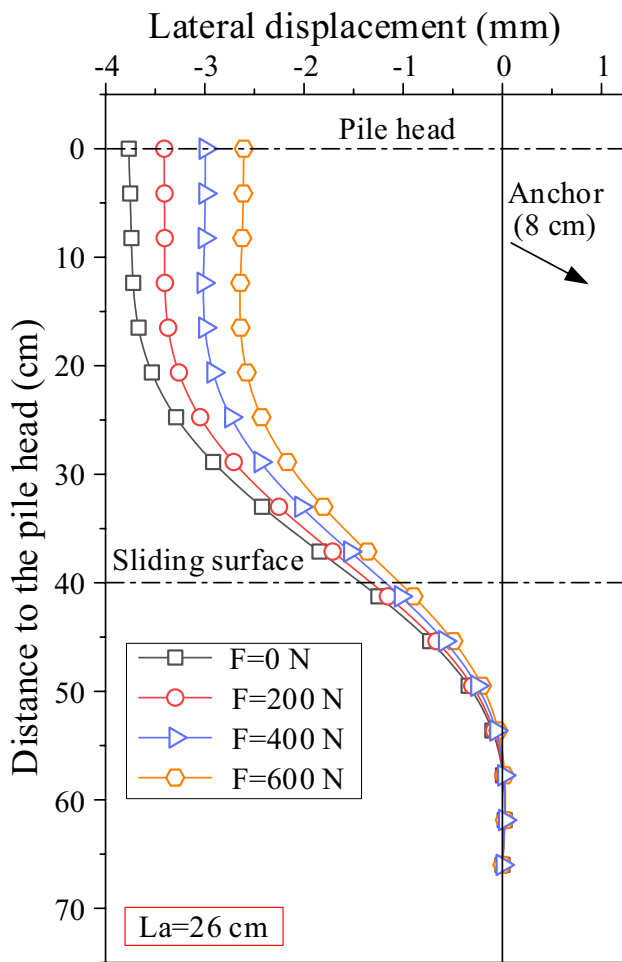


Fig. 19 Comparison of pile deflections with different initial prestresses of the anchor cables

Figure 20 shows the variation in the bending moment distribution of the pile with different initial prestresses of the anchor. In general, little change in the value and distribution of the pile bending moment occurred with the variation in the initial prestress. Specifically, the value of the bending moment in the pile decreases slightly with increasing initial prestress of the anchor. The maximum value of the positive bending moment decreases from 92.8 to 77.7 N·m when the initial prestress of the anchor increases from 0 to 600 N, while the maximum value of the negative bending moment decreases from -77.34 to -66.9 N·m. This finding demonstrates that the increase in the initial prestress of the anchor in a reasonable range can optimize the internal force in the piles to some extent.

Effect of the number of anchor levels

The first and second anchor levels locate at a distance of 8 and 16 cm from the pile head, respectively. The effects of

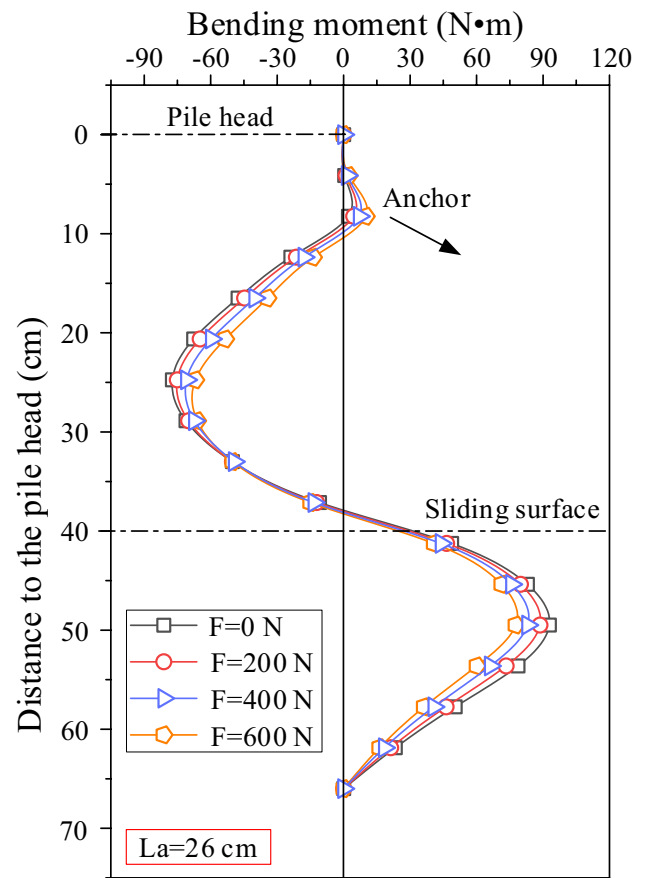


Fig. 20 Comparison of the bending moment in the piles with different initial prestresses of the anchor cable

the number of anchor levels on the pile deflection and bending moment are shown in Figs. 21 and 22, respectively. As shown in Fig. 21, the pile deflection tends to decrease with an increasing number of anchor levels, as expected, which is in agreement with the findings of anchored sheet pile walls by Wang (Wang et al. 2020). The corresponding absolute value of lateral displacements at the pile heads with different numbers of anchor levels (0, 1, and 2) are 24.68 mm, 3.41 mm, and 1.89 mm, respectively. It is evident that the maximum pile deflection experienced a sharp decrease from 25 to 3.5 mm as the number of anchor levels increases from 0 to 1, which indicates that the anchor plays a critical role in limiting the pile deformation.

As presented in Fig. 22, as the number of anchor levels increases, the maximum positive bending moment in the pile obviously decreases. The decrease in the maximum value of the positive bending moment can be as much as 63% (decreasing from 160.4 to 59.8 N·m) when the number of anchor levels increases from 0 to 2. In addition, it is observed that the bending moment distribution along the pile changes from spoon-shaped to S-shaped, with the number of

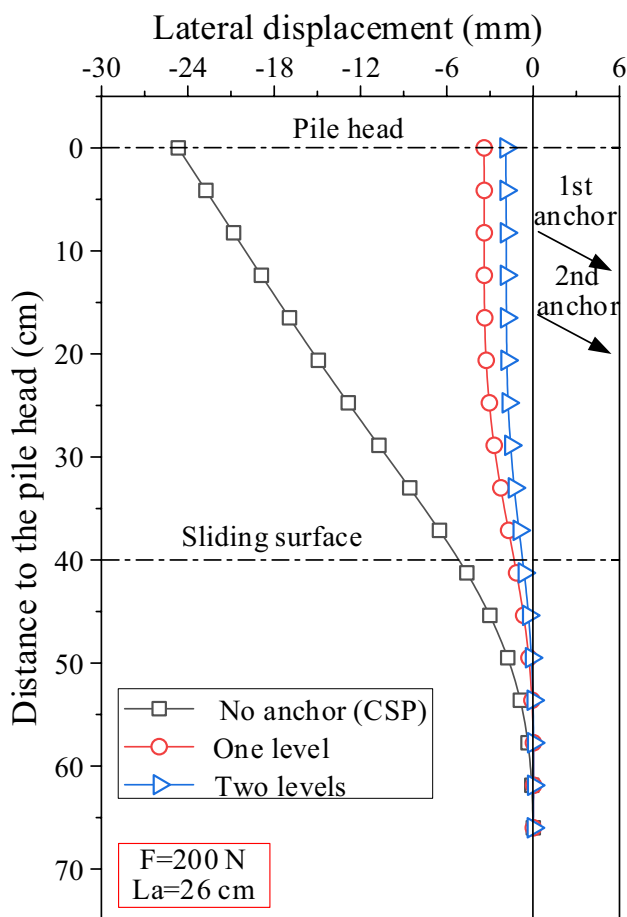


Fig. 21 Comparison of pile deflections with different numbers of anchor levels

anchor levels increasing from 0 to 1. These results indicate that the anchor can effectively amend the cantilever state of the pile and optimize the stress concentration near the sliding surface, which has also been validated under seismic conditions by other researchers (Huang et al. 2020a; Ma et al. 2019).

Discussion

Comparison with a model without anchor

A further comparison with another model without an anchor was conducted by numerical analysis. The ASP and CSP models represent landslides reinforced with ASPs and CSPs, respectively. A comparison of the pile deflection with two levels of thrust load at 10.8 and 12.0 kN of the ASP and CSP models is presented in Fig. 23. It is clear that the pile deflections in the CSP model are all obviously greater than those in the ASP model under two different levels of thrust load, especially for the lateral displacement at the pile head.

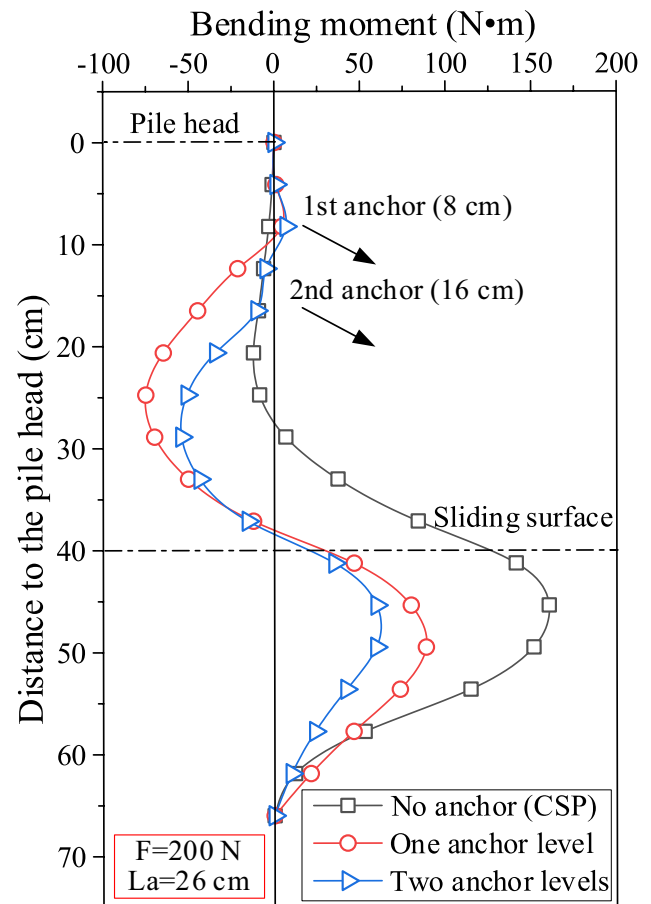


Fig. 22 Comparison of the bending moment in the piles with different numbers of anchor levels

This result further suggests that the deflection of piles can be well restrained in the ASP model due to the installation of the anchor.

Figure 24 shows a comparison of the variation rule in the safety factor during the entire progressive loading of the ASP and CSP model systems. In general, the evolution law of the safety factor in the ASP model is much different from that in the CSP model, especially when the landslide model is approaching instability. To be specific, in the ASP model, the safety factor experiences a sharp decrease during the initial loading stage and then is decreased gradually as a long process continues to decrease to 1.0. However, in the CSP model, the safety factor rapidly decreases at the initial loading and continues until the landslide model approaches failure. This behavior demonstrates that the failure of the landslide-ASP system is progressive, whereas that the landslide-CSP system may experience a sudden failure. Additionally, the safety factor for the CSP model is always smaller than that for the ASP model under the same thrust load. Meanwhile, the ASP model can sustain a higher thrust load (18.0 kN) than the CSP model (9.0 kN).

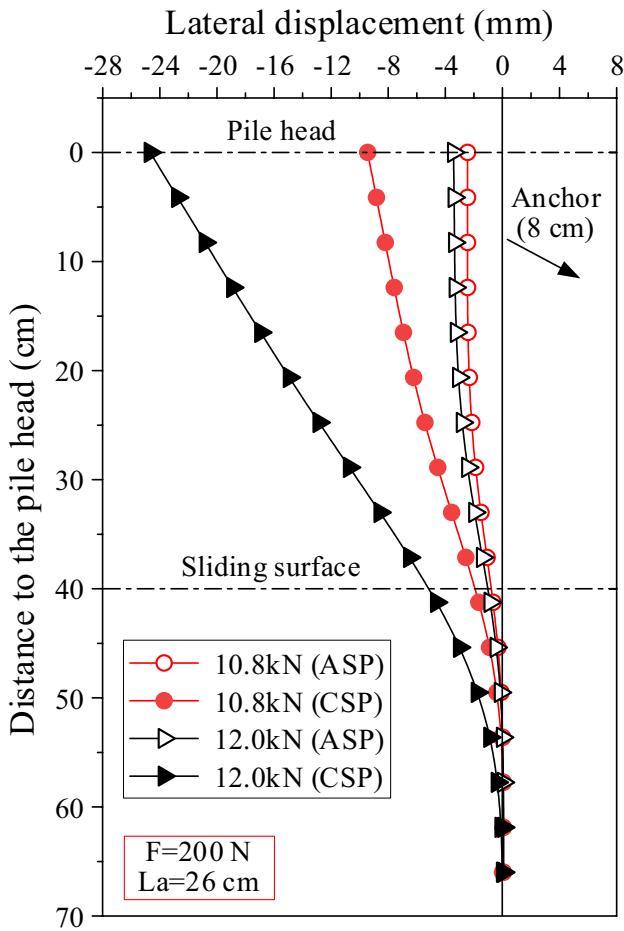


Fig. 23 Comparison of pile deflections for the ASP and CSP with two representative levels of the thrust load

Combined retaining mechanism of the stabilizing piles and anchor

To further understand the combined retaining mechanism of the stabilizing piles and prestressed anchor cable in landslides, the deformation and mechanical behaviors of the ASPs were analyzed in relation to the thrust load during landslide evolution. Figure 25 shows the variations in the lateral displacement at the pile head, maximum bending moment in the pile, maximum earth pressure behind the pile and anchor tension with the thrust load. In general, all curves have a similar trend and show three distinct phases. At the first loading phase, the maximum earth pressure on the pile increases only slightly due to the compaction of the soil between the pile and rigid thrust plate. In addition, it is also evident that the maximum bending moment increases with the maximum earth pressure, while the anchor tension is mobilized later due to the increase of the pile deflections. This behavior is because for the ASP, the stabilizing pile is a direct bearing structure, while the anchor is mobilized owing

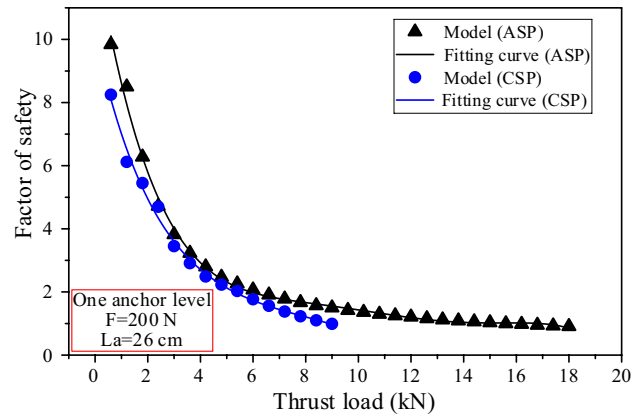


Fig. 24 Comparison of the evolution law of the factor of safety for the landslide-ASP and landslide-CSP systems during progressive loading

to pile deformation. With a further increase in thrust load, the maximum bending moment and the anchor tension all increase rapidly with increasing maximum earth pressure, which demonstrates that the increasing landslide thrust is borne by the stabilizing pile and anchor together after the anchor is mobilized, and finally transmitted to stable bed-rock to ensure the stability of the landslide. This finding also further indicates that the effectiveness of the ASPs to carry the landslide thrust is attributed to the combined effect of the stabilizing pile and anchor.

Based on the above analysis, it can be inferred that there is an adaptive dynamic balance process existing in the landslide-anchored stabilizing pile system subjected to the thrust load. Meanwhile, this is also the most superior feature of the ASPs over other stabilizing structures. Additionally, a sufficient safety reserve should be provided for the anchor in the design of an ASP to carry the increased anchor tension due to the increase in landslide thrust.

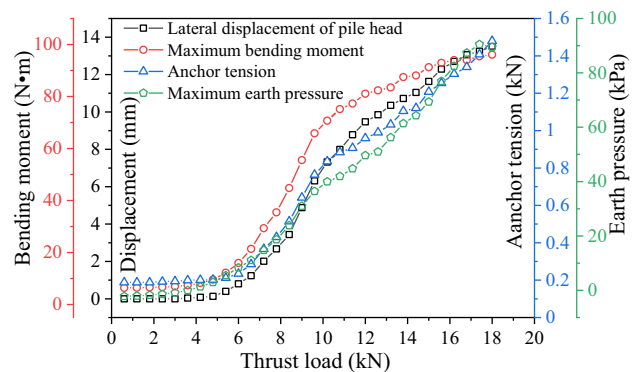


Fig. 25 The evolution laws of the maximum bending moment, maximum earth pressure, anchor tension, and lateral displacement at the pile head during progressive loading

Conclusions and future studies

In this paper, the behavior and retaining mechanism of ASPs in landslides were investigated by both a model test and numerical analysis. A 1:50 similitude ratio model test of landslide reinforced by ASPs under progressive loading was completed. In addition, a validated numerical model based on model test results was utilized to carry out the parametric study of ASPs. Furthermore, a comparison was made with results from a model without an anchor by numerical analysis, and the results show that compared with the CSP, the ASP can sustain higher thrust loads and better stabilize a landslide. Finally, the behaviors of the ASPs in relation to the thrust load were further analyzed and discussed to reveal the combined retaining mechanism of the stabilizing piles and prestressed anchor cable. The major conclusions are as follows:

1. The landslide thrust distribution behind the piles changes from a rectangular shape to a parabolic shape with a large top and a small bottom during progressive loading. The position of the maximum value of the landslide thrust moves upward with increasing thrust load on the rear of the model, which is a result of the inverse pulling effect of the anchor cable on the pile gradually increasing as the thrust load increases. The value of the earth's resistance is very small compared with that of the landslide thrust.
2. The bending moment in the pile is approximately S-shaped, and the maximum value of the positive bending moment occurs near the sliding surface. The variations in the maximum positive bending moment and anchor tension all show three distinct phases: stable, rapid growth, and slow increase, which reflects the dynamic mechanical characteristics of ASPs during landslide evolution.
3. The bending moment in the pile, anchor tension, and earth pressures behind the pile obtained from numerical analysis are generally consistent with the experimental results, which proves that the present numerical model is rational and effective for the analysis of the behavior of the ASPs in landslides.
4. There is a critical value (critical embedded pile length) regarding the influence of the embedded length of piles on the pile deflection and bending moment, which can achieve a balance between the pile behavior and economic benefit. The initial prestress of the anchor in a reasonable range can more effectively limit the deflections of the pile and optimize the internal force in the piles to some extent. The number of anchor levels has a significant effect on both the pile deflection and bending moment.
5. By comparing the differences in pile deflection and evolution law of the safety factor between the landslide-ASP and landslide-CSP systems, it was found that the ASP can sustain higher thrust loads and better stabilize the landslide than the CSP.
6. The combined retaining mechanism of the stabilizing piles and prestressed anchor cable can be summarized as follows: the landslide thrust is mainly carried by the pile initially, and the anchor tension is gradually mobilized with increasing earth pressure to share the landslide thrust together with the pile and transferred to stable bedrock to ensure the stability of the landslide.
7. Due to the prototype landslide has more complex conditions than the physical model test, and a half landslide model test is adopted in this study in the meantime, thus, the results obtained from the model tests are still difficult to directly applied to the prototype case.

Nevertheless, the influence of reservoir water was not considered in this study. Thus, more experiments will be conducted in the future to further investigate the long-term stability of landslide-ASP systems under reservoir conditions.

Funding This study was financially supported by the National Key R&D Program of China (2017YFC1501304) and China National Natural Science Foundation (41672314).

Declarations

Conflict of interest The authors declare no competing interests.

References

- Bilgin O (2010) Numerical studies of anchored sheet pile wall behavior constructed in cut and fill conditions. *Comput Geotech* 37:399–407. <https://doi.org/10.1016/j.compgeo.2010.01.002>
- Cai F (2017) A subgrade reaction solution for anchored dowel piles to stabilize landslides. In: *Advancing culture of living with landslides*, vol 3. *Advances in Landslide Technology*. https://doi.org/10.1007/978-3-319-53487-9_53
- Chen CY, Martin GR (2002) Soil-structure interaction for landslide stabilizing piles. *Comput Geotech* 29:363–386. [https://doi.org/10.1016/s0266-352x\(01\)00035-0](https://doi.org/10.1016/s0266-352x(01)00035-0)
- Dai Z (2002) Study on distribution laws of landslide-thrust and resistance of sliding mass acting on antislides piles. *Chin J Rock Mech Eng* 21:517–521
- Degrande G, Praet E, Van Zegbroeck B, Van Marcke P (2002) Dynamic interaction between the soil and an anchored sheet pile during seismic excitation. *Int J Numer Anal Meth Geomech* 26:605–631. <https://doi.org/10.1002/nag.214>
- Gazetas G, Garini E, Zafeirakos A (2016) Seismic analysis of tall anchored sheet-pile walls. *Soil Dyn Earthq Eng* 91:209–221. <https://doi.org/10.1016/j.soildyn.2016.09.031>
- Ghasemzadeh H, Tarzaban M, Hajitaheriha MM (2018) Numerical analysis of pile–soil–pile interaction in pile groups with batter

- piles. *Geotech Geol Eng* 36:2189–2215. <https://doi.org/10.1007/s10706-018-0456-4>
- Guo W, Qin H (2010) Thrust and bending moment of rigid piles subjected to moving soil. *Canadian Geotech J* 47:180–196. <https://doi.org/10.1139/T09-092>
- He Y, Hazarika H, Yasufuku N, Teng J, Jiang Z, Han Z (2015) Estimation of lateral force acting on piles to stabilize landslides. *Nat Hazards* 79:1981–2003. <https://doi.org/10.1007/s11069-015-1942-0>
- He C, Hu X, Tannant DD, Tan F, Zhang Y, Zhang H (2018) Response of a landslide to reservoir impoundment in model tests. *Eng Geol* 247:84–93. <https://doi.org/10.1016/j.enggeo.2018.10.021>
- He C, Hu X, Liu D, Xu C, Wu S, Wang X, Zhang H (2020) Model tests of the evolutionary process and failure mechanism of a pile-reinforced landslide under two different reservoir conditions. *Eng Geol*. <https://doi.org/10.1016/j.enggeo.2020.105811>
- Hu X, Zhou C, Xu C, Liu D, Wu S, Li L (2019) Model tests of the response of landslide-stabilizing piles to piles with different stiffness. *Landslides* 16:2187–2200. <https://doi.org/10.1007/s10346-019-01233-4>
- Huang Y, Xu X, Liu J, Mao W (2020a) Centrifuge modeling of seismic response and failure mode of a slope reinforced by a pile-anchor structure. *Soil Dyn Earthq Eng*. <https://doi.org/10.1016/j.soildyn.2020.106037>
- Huang Y, Xu X, Mao W (2020b) Numerical performance assessment of slope reinforcement using a pile-anchor structure under seismic loading. *Soil Dyn Earthq Eng*. <https://doi.org/10.1016/j.soildyn.2019.105963>
- ITASCA Consulting Group I (2012) User manual for FLAC3D, version.5.0. Itasca Consulting Group Inc, Minnesota
- Jia GW, Zhan TLT, Chen YM, Fredlund DG (2009) Performance of a large-scale slope model subjected to rising and lowering water levels. *Eng Geol* 106:92–103. <https://doi.org/10.1016/j.enggeo.2009.03.003>
- Jian W, Xu Q, Yang H, Wang F (2014) Mechanism and failure process of Qianjiangping landslide in the three gorges reservoir. *China Environ Earth Sci* 72:2999–3013. <https://doi.org/10.1007/s12665-014-3205-x>
- Kahyaoglu MR, İmançlı G, Özden G, Kayalar AŞ (2017) Numerical simulations of landslide-stabilizing piles: a remediation project in Söke, Turkey. *Environ Earth Sci* 76:656. <https://doi.org/10.1007/s12665-017-6989-7>
- Kang G-C, Song Y-S, Kim T-H (2009) Behavior and stability of a large-scale cut slope considering reinforcement stages. *Landslides* 6:263–272. <https://doi.org/10.1007/s10346-009-0164-5>
- Li C et al (2016) Model testing of the response of stabilizing piles in landslides with upper hard and lower weak bedrock. *Eng Geol* 204:65–76. <https://doi.org/10.1016/j.enggeo.2016.02.002>
- Li S, Sun Q, Zhang Z, Luo X (2018) Physical modelling and numerical analysis of slope instability subjected to reservoir impoundment of the three gorges. *Environ Earth Sci*. <https://doi.org/10.1007/s12665-018-7321-x>
- Lin M, Wang K (2006) Seismic slope behavior in a large-scale shaking table model test. *Eng Geol* 86: 118–133. <https://doi.org/10.1016/j.enggeo.2006.02.011>
- Ling H, Ling HI (2012) Centrifuge model simulations of rainfall-induced slope instability. *J Geotech Geoenviron Eng* 138:1151–1157. [https://doi.org/10.1061/\(asce\)gt.1943-5606.0000679](https://doi.org/10.1061/(asce)gt.1943-5606.0000679)
- Lirer S (2012) Landslide stabilizing piles: experimental evidences and numerical interpretation. *Eng Geol* 149:70–77. <https://doi.org/10.1016/j.enggeo.2012.08.002>
- Liu D, Hu X, Zhou C, Xu C, He C, Zhang H, Wang Q (2020) Deformation mechanisms and evolution of a pile-reinforced landslide under long-term reservoir operation. *Eng Geol*. <https://doi.org/10.1016/j.enggeo.2020.105747>
- Liu S, Luo F, Zhang G (2021) Pile reinforcement behavior and mechanism in a soil slope under drawdown conditions. *Bull Eng Geol Environ*. <https://doi.org/10.1007/s10064-021-02191-9>
- Ma N, Wu H, Ma H, Wu X, Wang G (2019) Examining dynamic soil pressures and the effectiveness of different pile structures inside reinforced slopes using shaking table tests. *Soil Dyn Earthq Eng* 116:293–303. <https://doi.org/10.1016/j.soildyn.2018.10.005>
- Paronuzzi P, Rigo E, Bolla A (2013) Influence of filling-drawdown cycles of the Vajont reservoir on Mt. Toc slope stability. *Geomorphology* 191:75–93. <https://doi.org/10.1016/j.geomorph.2013.03.004>
- Qu H-L, Luo H, Hu H-G, Jia H-Y, Zhang D-Y (2018) Dynamic response of anchored sheet pile wall under ground motion: analytical model with experimental validation. *Soil Dyn Earthq Eng* 115:896–906. <https://doi.org/10.1016/j.soildyn.2017.09.015>
- Shen Y, Yu Y, Ma F, Mi F, Xiang Z (2017) Earth pressure evolution of the double-row long-short stabilizing pile system. *Environ Earth Sci*. <https://doi.org/10.1007/s12665-017-6907-z>
- Smethurst JA, Powrie W (2007) Monitoring and analysis of the bending behaviour of discrete piles used to stabilise a railway embankment. *Geotechnique* 57:663–677. <https://doi.org/10.1680/geot.2007.57.8.663>
- Song H, Cui W (2016) A large-scale colluvial landslide caused by multiple factors: mechanism analysis and phased stabilization. *Landslides* 13:321–335. <https://doi.org/10.1007/s10346-015-0560-y>
- Song Y-S, Hong W-P, Woo K-S (2012) Behavior and analysis of stabilizing piles installed in a cut slope during heavy rainfall. *Eng Geol* 129:56–67. <https://doi.org/10.1016/j.enggeo.2012.01.012>
- Tan H, Jiao Z, Chen J (2018) Field testing and numerical analysis on performance of anchored sheet pile quay wall with separate pile-supported platform. *Mar Struct* 58:382–398. <https://doi.org/10.1016/j.marstruc.2017.12.006>
- Tang H, Hu X, Xu C, Li C, Yong R, Wang L (2014) A novel approach for determining landslide pushing force based on landslide-pile interactions. *Eng Geol* 182:15–24. <https://doi.org/10.1016/j.enggeo.2014.07.024>
- Tang H, Wasowski J, Juang CH (2019) Geohazards in the three Gorges Reservoir Area, China: lessons learned from decades of research. *Eng Geol* 2:61. <https://doi.org/10.1016/j.enggeo.2019.105267>
- Wang C, Wang H, Jiao Y, Qin W, Tian H (2020) Optimal design of a high slope for Ice World and Water Park (IWWP) built over an abandoned quarry: a case study in Changsha of China. *Geotech Geol Eng*. <https://doi.org/10.1007/s10706-020-01550-9>
- Wu F, Luo Y, Chang Z (2011) Slope reinforcement for housing in Three Gorges reservoir area. *J Mt Sci* 8:314–320. <https://doi.org/10.1007/s11629-011-2109-4>
- Wu R, Zhou H, Hu Y, Zhong Y, Li P, Yang J (2015) An improved method for calculating anti-sliding pile with prestressed anchor cable based on finite difference theory. *Rock Soil Mech* 36:1791–1800
- Xu X, Huang Y (2021) Parametric study of structural parameters affecting seismic stability in slopes reinforced by pile-anchor structures. *Soil Dynamics and Earthquake Engineering* 147:106789. <https://doi.org/10.1016/j.soildyn.2021.106789>
- Yang S, Ren X, Zhang J (2011) Study on embedded length of piles for slope reinforced with one row of piles. *J Rock Mech Geotech Eng* 3:167–178. <https://doi.org/10.3724/SP.J.1235.2011.00167>
- Zekri A, Ghalandarzadeh A, Ghasemi P, Aminfar MH (2015) Experimental study of remediation measures of anchored sheet pile quay walls using soil compaction. *Ocean Eng* 93:45–63. <https://doi.org/10.1016/j.oceaneng.2014.11.002>
- Zhang G, Wang LP, Wang YL (2017) Pile reinforcement mechanism of soil slopes. *Acta Geotech* 12:1035–1046. <https://doi.org/10.1007/s11440-017-0543-3>

- Zhang Y, Hu X, Tannant DD, Zhang G, Tan F (2018) Field monitoring and deformation characteristics of a landslide with piles in the Three Gorges Reservoir area. *Landslides* 15:581–592. <https://doi.org/10.1007/s10346-018-0945-9>
- Zhao B, Wang Y-S, Wang Y, Shen T, Zhai Y-C (2017) Retaining mechanism and structural characteristics of h type anti-slide pile (hTP pile) and experience with its engineering application. *Eng Geol* 222:29–37. <https://doi.org/10.1016/j.enggeo.2017.03.018>
- Zhao G, Yang Y, Zhang H, Zhang G (2019a) A case study integrating field measurements and numerical analysis of high-fill slope stabilized with cast-in-place piles in Yunnan, China. *Eng Geol* 253:160–170. <https://doi.org/10.1016/j.enggeo.2019.03.005>
- Zhao W, Du C, Sun L, Chen X (2019b) Field measurements and numerical studies of the behaviour of anchored sheet pile walls constructed with excavating and backfilling procedures. *Eng Geol*. <https://doi.org/10.1016/j.enggeo.2019.105165>
- Zhong Z, Yong R, Tang H, Li C, Du S (2020) Experimental studies on the interaction mechanism of landslide stabilizing piles and sandwich-type bedrock. *Landslides*. <https://doi.org/10.1007/s10346-020-01570-9>
- Zhou C, Hu X-l, Zheng W-B, Xu C, Wang Q (2020) Displacement characteristic of landslides reinforced with flexible piles: field and physical model test. *J Mt Sci* 17:787–800. <https://doi.org/10.1007/s11629-019-5743-x>
- Zhou C, Shao W, van Westen CJ (2014) Comparing two methods to estimate lateral force acting on stabilizing piles for a landslide in the Three Gorges Reservoir, China. *Eng Geol* 173:41–53. <https://doi.org/10.1016/j.enggeo.2014.02.004>